

# Evaluation of Regional Elevation and Blade Density Effects on the Efficiency of a 1-kW Wind Turbine for Operation in Low-Wind Counties in Iran

Vahid Akbari <sup>1</sup>, Mohammad Naghashzadegan <sup>2,\*</sup>, Ramin Kouhikamali <sup>3</sup> and Wahiba Yaïci <sup>4</sup>

<sup>1</sup> Mechanical Engineering Department, University Campus 2, University of Guilan, Rasht 4144784475, Iran; v4\_akbari@yahoo.com

<sup>2</sup> Mechanical Engineering Department, University of Guilan, Rasht 4199613776, Iran

<sup>3</sup> Mechanical Engineering Department, Isfahan University of Technology, Isfahan 8415683111, Iran; r.kouhikamali@iut.ac.ir

<sup>4</sup> CanmetENERGY Research Centre, Natural Resources Canada, Ottawa, ON K1A 1M1, Canada; wahiba.yaici@nrcan-rncan.gc.ca

\* Correspondence: naghash@guilan.ac.ir

**Abstract:** This research investigates the effect of blade density and elevation above sea level on the startup time ( $T_s$ ) and power coefficient ( $C_p$ ) of a 1-kW two-bladed wind turbine. The study uses three Iranian hardwoods as the blade material and four counties of Iran with low wind speeds and different elevations as the case studies. The BW-3 airfoil is considered as the blade profile. A multi-objective optimization process with the aid of the differential evolution (DE) algorithm is utilized to specify the chord length and twist angle. The findings demonstrate that, while the maximum  $C_p$  of the optimal blades designed with all three types of wood is high and equal to 0.48, the average  $T_s$  of the optimal blades designed with oak and hornbeam wood is 84% and 108% higher than that of alder wood, respectively. It is also observed that, while raising the elevation to 2250 m decreases the  $C_p$  by only 2.5%, the ideal blade designed to work at sea level could not manage to start rotating at a height of 1607 m and above. Finally, an improvement in the  $T_s$  and  $C_p$  was observed by performing optimization based on the local atmospheric conditions associated with the incrementing blade chord length at high elevations.

**Keywords:** renewable energy; small wind turbine; wind energy; blade material; elevation; timber blade; startup behavior; DE optimization; power coefficient; Iran



**Citation:** Akbari, V.; Naghashzadegan, M.; Kouhikamali, R.; Yaïci, W.

Evaluation of Regional Elevation and Blade Density Effects on the Efficiency of a 1-kW Wind Turbine for Operation in Low-Wind Counties in Iran. *Wind* **2023**, *3*, 320–342. <https://doi.org/10.3390/wind3030019>

Academic Editors: Wenzhong Shen and Francesco Castellani

Received: 8 June 2023

Revised: 6 August 2023

Accepted: 10 August 2023

Published: 11 August 2023



**Copyright:** © 2023 by the authors. Licensee MDPI, Basel, Switzerland. This article is an open access article distributed under the terms and conditions of the Creative Commons Attribution (CC BY) license (<https://creativecommons.org/licenses/by/4.0/>).

## 1. Introduction

After the oil crisis and the spike in fossil fuel prices in the 1970s, the next big shock to the global energy market was undoubtedly the Russia–Ukraine conflict. Efforts to accelerate the shift towards renewable energy have never been more serious [1]. Thus, the possibility of the prominence of renewable energies, especially wind energy, and the phasing out of fossil fuels has been greatly strengthened [2]. In this regard, Germany, which is the third-most producer of wind power in the world, presented a plan to produce 100% of its energy from renewable sources by 2035 [3]. Moreover, the European Union aims to meet 50% of its energy demand through wind by 2050 [4]. With a straightforward structure, minimalistic design, easy portability, and reduced noise, small wind turbines (SWTs) have become indispensable tools for harnessing wind energy in rural, suburban, and even densely populated urban areas, where installing large wind turbines (LWTs) is impractical due to limited space and noise concerns [5].

Different methods have been developed to analyze the flow around wind turbine (WT) blades, calculate the aerodynamic torque ( $M$ ), and as a result, compute the output power of turbines, the most important of which are experimental testing in the wind tunnel, the blade element momentum (BEM) method, and the computational fluid dynamics

(CFD) simulations. While the first technique provides real data, it is often time-consuming and costly. In contrast, both the BEM theory and CFD technique offer the advantage of generating varied and trustable results at a reduced expense. Refan and Hangan [6] conducted both experimental and theoretical assessments on the aerodynamic behavior of a small 2.2-m diameter upwind three-bladed horizontal axis wind turbine (HAWT) rotor. Their comparison of the theoretical and experimental findings indicated that the overall predictions of the BEM theory fall within an acceptable accuracy range. Plaza et al. [7] carried out an aerodynamic evaluation of the MEXICO WT rotor, comparing the data from the BEM theory, CFD analysis, and experimental tests. Their findings revealed that, at lower wind speeds ( $V$ ), the BEM theory presents more reliable data than the the CFD analysis.

The wind is turbulent by nature, and its turbulence is considered to be the result of friction with the Earth's topography and the nonuniform heating of different air layers above the ground. Turbulence refers to the variation in wind speed around its average value over a particular period. This period can be annually, daily, or for periods less than 10 min. It is a complex phenomenon to describe accurately, so it is usually represented by a statistical property known as turbulence intensity. Turbulence intensity ( $I$ ) can be computed by dividing the standard deviation ( $\sigma$ ) of wind speeds by the mean wind speed ( $U$ ) over a particular period (Equation (1)) [8]:

$$I = \frac{\sigma}{U} \quad (1)$$

This intensity varies from about 0.1 (10%) for smooth terrain to more than 0.2 (20%) for rough terrain [9]. It has been shown that high turbulence intensity is the main factor that shortens the fatigue life of a turbine structure [10], and it also affects the furling behavior [11]. Many mathematical models can describe atmospheric turbulence. Some models, like those usually used in CFD simulations, are time-dependent. Other techniques work based on the frequency domain [12,13].

The influence of turbulence on the power output is challenging to generalize, since furling/power limiting, airfoil performance, and wind alignment are influenced by turbulent gusts. Winds with higher turbulence intensities have higher power than winds with less turbulence but the same mean wind speed because of the cubic variation of power with the wind speed.

The research studies by Churchfield et al. [14] and Nandi et al. [15] showed that, in large wind turbines, the oncoming atmospheric turbulence can result in considerable fluctuations in the local angles of attack and their aerodynamic performance. However, based on research studies on small wind turbines with operating Reynolds numbers less than 500,000, the influence of atmospheric turbulence on their aerodynamic performance is not significant [9,16]. In this regard, Lubitz [17] experimentally evaluated the influence of atmospheric turbulence on the output power of a Bergey XL.1 1-kW small wind turbine. This turbine, which used a BW-3 airfoil as its blade profile, was installed 18 m above the ground. The results of this study showed that the turbulence levels had an insignificant influence on the overall power output at wind speeds between the startup and furling. Based on their findings for the normal operating range (4 m/s to 7 m/s), while a low turbulence intensity ( $I < 0.14$ ) resulted in only a 2% reduction in the power output relative to the power output over all turbulence conditions, medium and high turbulence intensities ( $I > 0.14$ ) led to a power rise of around 2%. In another research, Wood [9] assessed the influence of atmospheric turbulence on the performance of a small wind turbine. For this purpose, he analyzed the daily output of two identical Skystream 2.4-kW small wind turbines over 16 days (30 April–15 May). These turbines were installed on towers 11 m in the city of Calgary, Canada, at a distance 8 km from each other. The first turbine was installed on flat ground around 80 m away from a large two-story house, and the second turbine was installed at the same distance from a similarly sized house but on a ridge. Despite the differences in these sites and the variation in atmospheric turbulence they caused, the average power outputs of these turbines were found to be 12.62 kWh

and 12.91 kWh, respectively (2.24% difference). Therefore, overall, the literature review indicates that, unlike large wind turbines [13–15], atmospheric turbulence does not have a significant influence on the output power of small wind turbines with Reynolds numbers less than 500,000 [9,17], and it mostly affects the structure fatigue life [10] and furling behavior [11] in these turbines.

Due to the laminar separation that occurs at low Reynolds numbers, the aerodynamics of wind turbines operating at low wind speeds is challenging. At Reynolds numbers below  $5 \times 10^5$ , the flow around an airfoil might separate while the boundary layer is still laminar and before the transition to turbulent. This laminar separation might lead to the formation of air bubbles, which are known as laminar separation bubbles. These bubbles result in extra drag in airfoils, which is defined by the bubble drag. Figure 1 shows a schematic of laminar separation bubbles. A typical airfoil not designed for operating at low Reynolds numbers will suffer from a loss in performance in this condition; however, some thin airfoils are designed to operate at low Reynolds numbers and reduce the impact of the separation bubble. The BW-3 airfoil is one of these airfoils [18].

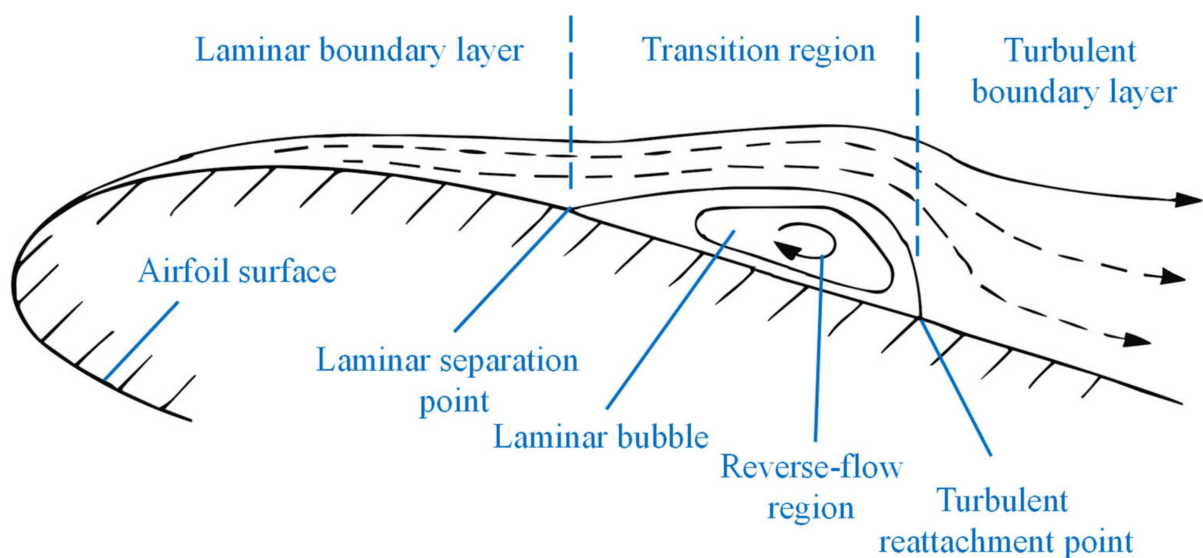


**Figure 1.** The schematic of a laminar separation bubble.

In this regard, the design and optimization of small wind turbine blades with the help of the BEM method using the experimental lift and drag coefficients of thin airfoils has provided accurate results and has received much attention from researchers in recent years [19–21]. The current research is based on this method as well.

To enhance the lift-to-drag coefficient and elevate the performance of an airfoil with applications in wind turbines, Liu et al. [22] worked on the transition of the boundary layer and its effects on the stall performance. They made use of the CFD method for simulating the transition over an airfoil in pitching movement. They stated that the transition model exhibits more accurate predictions than the conventional turbulence model in light dynamic stalls. Nandi et al. [23] used a numerical method based on the BEM and the unsteady Reynolds-averaged Navier–Stokes (URANS) to focus on the transitional boundary layers to investigate the influence of transient atmospheric conditions that are exerted on the turbine blades. The capability of this method was compared against the SST  $k-\omega$  model. According to the findings, the transition model was more successful in predicting the dynamics of the boundary layer. Also, this method outperformed the SST  $k-\omega$  model for capturing the lift curve.

Not using pitch and yaw control mechanisms is the most important difference between SWTs and LWTs [24]. With the aid of the pitch mechanism, the blade rotates around its longitudinal axis, and by changing the twist angle, efforts are made to keep the value of the angle of attack (AOA) at the desired level. The yaw mechanism rotates the turbine when the direction of the wind changes, and it puts the turbine directly in front of the wind [25]. Unlike LWTs, SWTs do not have the yaw mechanism. In SWTs, a mechanical system called a tail fin is used instead. It should be explained that, based on standards, an SWT has a rated power of less than 50 kW, which corresponds to a blade length of less than 8 m [26]. In a more detailed classification, SWTs are classified into three groups: micro ( $\leq 1$  kW), medium ( $\leq 5$  kW), and mini ( $\leq 50$  kW) [18]. The second difference between SWTs and LWTs is the number of airfoils used in the blade. To reduce the manufacturing cost of SWT blades, only one airfoil is used all over the blade, but in LWT blades, the operating conditions of the root and tip sections are completely different from each other. In the root section of LWT blades, considerable bending moments occur, which requires the use of thick airfoils. Thinner airfoils, which have superior aerodynamic behavior, are utilized in the middle and tip sections to harness more energy from the wind [27]. Since the main goal of designing a WT is to acquire the maximum power output, the way that this parameter is considered in the blade design process can be counted as the third main difference between SWTs and LWTs. LWTs are installed in windy regions, so their design and optimization are not based on a specific speed but based on reaching the maximum annual energy production (AEP) in a range of various speeds. On the other hand, SWTs are installed in places that do not have good wind potential [28], requiring maximum efficiency for the turbine during the limited instances in which the wind is blowing. Thus, the power coefficient ( $C_p$ ) is employed to design the blades of these turbines [29].

At low  $V$  values, the startup process of SWTs is delayed, and the generation of power is more idle [30]. The main reason is the absence of a pitch control mechanism. Also, permanent magnet generators (PMGs) used in SWTs have a high cogging torque ( $M_c$ ) that must be overcome by the generated startup torque ( $M_s$ ) [19]. Studies have shown that the  $M$  values generated by the root elements of the blade have a vital role in starting the blade rotation from the stationary state, and the startup process of the blade is mostly contributed by these elements. As the rotational speed of the turbine rises, the AOA along the blade reduces, so that the aerodynamic moment generated by the elements near the blade tip is much larger than that of the root elements. Thus, these elements have a greater contribution to the amount of power output from the turbine.

In SWTs, after choosing the airfoil type utilized in the blade, the twist angle ( $\beta$ ) and the chord length ( $c$ ) in each blade element can be computed by the Schmitz equations [31]:

$$\beta = \frac{2}{3} \tan^{-1} \left( \frac{1}{\lambda_r} \right) - \alpha \quad (2)$$

$$c = \frac{16\pi r}{BC_l} \sin^2 \left( \frac{1}{3} \tan^{-1} \left( \frac{1}{\lambda_r} \right) \right) \quad (3)$$

In these equations,  $\lambda_r$  is the local tip speed ratio,  $\alpha$  is the AOA in which the lift-to-drag ratio is the maximum,  $B$  is the number of blades, and  $C_l$  is the lift coefficient. Research studies have suggested that, while using the nonlinear distribution obtained from Equations (2) and (3) provides the maximum  $C_p$ , it causes a significant reduction in the  $M_s$  and therefore leads to an increment in the rotor startup time [32]. Similar results have been presented for the application of the ideal equations provided by Burton et al. [33] for the design of SWT blades [34]. Thus, if any other objectives besides the  $C_p$  are considered for the blade design, optimization methods should be employed [35]. In general, optimization techniques fall into two groups: gradient, and nongradient [36]. In gradient techniques, the derivative of the objective function with respect to the design variables is acquired, and then, the optimization process is carried out using them. The solving techniques of adjoint [37] and second-order sequential quadratic equations [38], as well as the finite

difference method [39], are some of the gradient techniques. Nongradient methods are independent from the objective function characteristics, such as continuity and differentiability. In this regard, the optimal solution is determined by calculating the values of the objective function and comparing to with each other in an evolutionary process. Genetic algorithm (GA) [40], differential evolution (DE) [41], and particle swarm optimization (PSO) [42] are among the most famous nongradient algorithms. Robustness, rapidness, and convergence rate are the most fundamental features of the optimization methods, in which evolutionary algorithms, especially the DE algorithm, have been very successful [43].

Akbari et al. [32] designed and optimized the blades of an SWT with a blade length of 1.5 m by using the NACA4412 airfoil as the blade section to increase the  $M_s$ . By raising the  $\beta$  and the  $c$  at  $r/R < 0.52$  and following the Schmitz formula at  $r/R \geq 0.52$ , they managed to obtain a 140% increment in the  $M_s$  by losing only 1.5% of the  $C_p$  value. This resulted in reducing the startup speed from 6 to 4 m/s. Pourrajabian et al. [44] investigated the chord and twist variables in three SWTs with power outputs of 0.5, 0.75, and 1 kW. They focused on enhancing the turbines' operation during low wind conditions at the startup time. Enlarging the  $c$  and  $\beta$  values at the root section of the blades was found to be essential for reaching a better performance in low-wind scenarios. Their findings indicate that using more blades or enlarging the existing ones contributes to both a better startup process and greater power generation. Abdelsalam et al. [45] conducted experimental research on the aerodynamic efficiency of two distinct small HAWT rotors. The first rotor possessed nonlinear chord and twist distributions, while the second one had a novel linearized pattern that was designed using the BEM theory. The RISØ-A-24 airfoil was used as the blade profile. The findings exhibited that the maximum  $C_p$  of the nonlinear model was higher; however, the linear model had a better startup performance. In the study carried out by Rahgozar et al. [21], a one-meter wooden HAWT blade was developed by taking both the startup time and power output into account. They tested four potential combinations of linear/nonlinear  $c$  and  $\beta$  distributions utilizing the BEM theory. They made use of the SG6043 airfoil as the uniform profile along the blade. They concluded that employing a linear distribution enhances the startup performance with a minimal impact on the power output. By choosing ten airfoils that are prominently used in the SWT industry, Akbari et al. [34] recommended the application of Bergye BW-3 and SG6043 airfoils as blade profiles for use in less and more windy regions, respectively. The reduced inertia presented in the blades featuring the Bergye BW-3 profile, along with the impressive lift-to-drag proportion exhibited by the SG6043 design, represent some of the noteworthy benefits of these aerodynamic structures.

As compared to LWTs, the blades of SWTs are manufactured from more diverse materials and methods. Glass fiber and carbon fiber reinforcement embedded in epoxy are the most prevalent materials that are used for manufacturing LWTs [46]. Although the material technology of large blades can be applied to small blades, they are typically costly and are associated with a substantial growth of manufacturing expenses. Studies have shown that paying attention to fatigue is cardinal in SWTs [47]. Wood is used as a stable, green, inexpensive, and durable engineering material in a wide range of devices, such as airplane propellers and SWT blades. The fatigue resistance of wood is excellent, and the strength-to-density ratio of this material is very satisfactory [48]. In this regard, research has shown that wood has applications for manufacturing SWT blades that have a capacity of 5 kW or less and a length of no more than 2.5 m [49]. Blade and air densities are important parameters in the startup behavior of SWTs, which affect the blade inertia and the  $M_s$ , respectively. On the other hand, with the rise in elevation and the kinematic viscosity of the air, the Reynolds number ( $Re$ ) on the blade is reduced and can decrease the lift value and, as a result, decrease the  $C_p$  of the turbine. Considering the increase in the application of SWTs and the requirement to improve their performance, especially at low  $V$  values, the importance of these parameters can be well perceived. For this purpose, in the current study, three hardwoods with different densities that grow in Iran and also four low-wind counties with different elevations from the sea level up to 2250 m were selected

as case studies. In the subsequent sections of the study, by designing and optimizing a low-cost two-bladed SWT, the impact of the blade density and elevation on the startup behavior and the power extraction coefficient will be investigated.

## 2. Wind and Timber Resources in Iran

Iran, a historic nation in the Middle East, is placed between Africa, Europe, and Asia. As the 17th largest nation globally, Iran shares borders with Afghanistan and Pakistan to the east; Armenia, Turkmenistan, and Azerbaijan to the north (and the Caspian Sea); Iraq, and Turkey to the west; and the Sea of Oman, as well as the Persian Gulf, to the south.

Iranians are pioneers in using wind energy to pump water and grind grains. The first windmill was used around 644 B.C. in Sistan, Iran [50]. Despite being situated in a wind-rich region and possessing substantial wind energy potential, Iran has merely harnessed 342 MW of its wind capacity by 2023, which is a small contribution to supplying Iran's 90 GW electricity requirement [51]. Natural gas is the largest source of electricity supply in Iran, which includes about 81% of the total production, followed by oil and hydro at 14 and 4%, respectively [51]. While the conducted studies show the potential of at least 18 GW of wind energy in Iran [52], the share of wind energy in Iran's energy portfolio has always been less than 0.5% [52], while the corresponding average value in the world is virtually 6.5% [53]. Therefore, it is evident that further efforts are required to tap into Iran's wind energy resources. The wind energy potential has been investigated in some regions of Iran, including Bushehr [54], Zahedan [55], Tabriz and Ardabil [56], Tehran [57], Zanjan [58], Chalus [59], and Semnan [60]. Also, Mostafaeipour [61] evaluated the practicality of deploying offshore WTs in the Persian Gulf and the Caspian Sea.

To assess the impact of elevation on the aerodynamic efficiency of SWTs, four counties with different elevations were considered, according to Table 1. In this table, the air properties are determined based on the International Standard Atmosphere (ISA) [62].

**Table 1.** Specifications of the considered counties.

Case Study	County	Elevation (m)	Air Density (kg/m <sup>3</sup> )	Air Kinematic Viscosity (m <sup>2</sup> /s)	Coordinate E–N
Sea level	-	0	1.225	$1.460 \times 10^{-5}$	-
1	Dalgan	392	1.1795	$1.525 \times 10^{-5}$	59°32'–27°26'
2	Maku	1182	1.0919	$1.624 \times 10^{-5}$	44°38'–39°29'
3	Asadabad	1607	1.0468	$1.680 \times 10^{-5}$	48°8'–34°47'
4	Sisakht	2250	0.9814	$1.771 \times 10^{-5}$	51°45'–30°86'

The locations of the selected cities are shown in Figure 2a, with numbers 1 to 4 for Dalgan, Maku, Asadabad, and Sisakht, respectively. Iran is home to various forest types, particularly in the western and northern regions. The Caspian Hyrcanian forests in Northern Iran span 1.8 million hectares, extending from the Caspian Sea coastline to an elevation of 2800 m above sea level on the northern slopes of the Alborz Mountain Range (Figure 2b). Due to the mild, humid climate and suitable soil, these forests produce more than 900,000 m<sup>3</sup> of wood annually [63]. In the present study, three types of hardwood grown in this area, namely alder, oak, and hornbeam, which physical properties were presented in the work of Kiaei and Samariha [64], were used for the SWT blades.

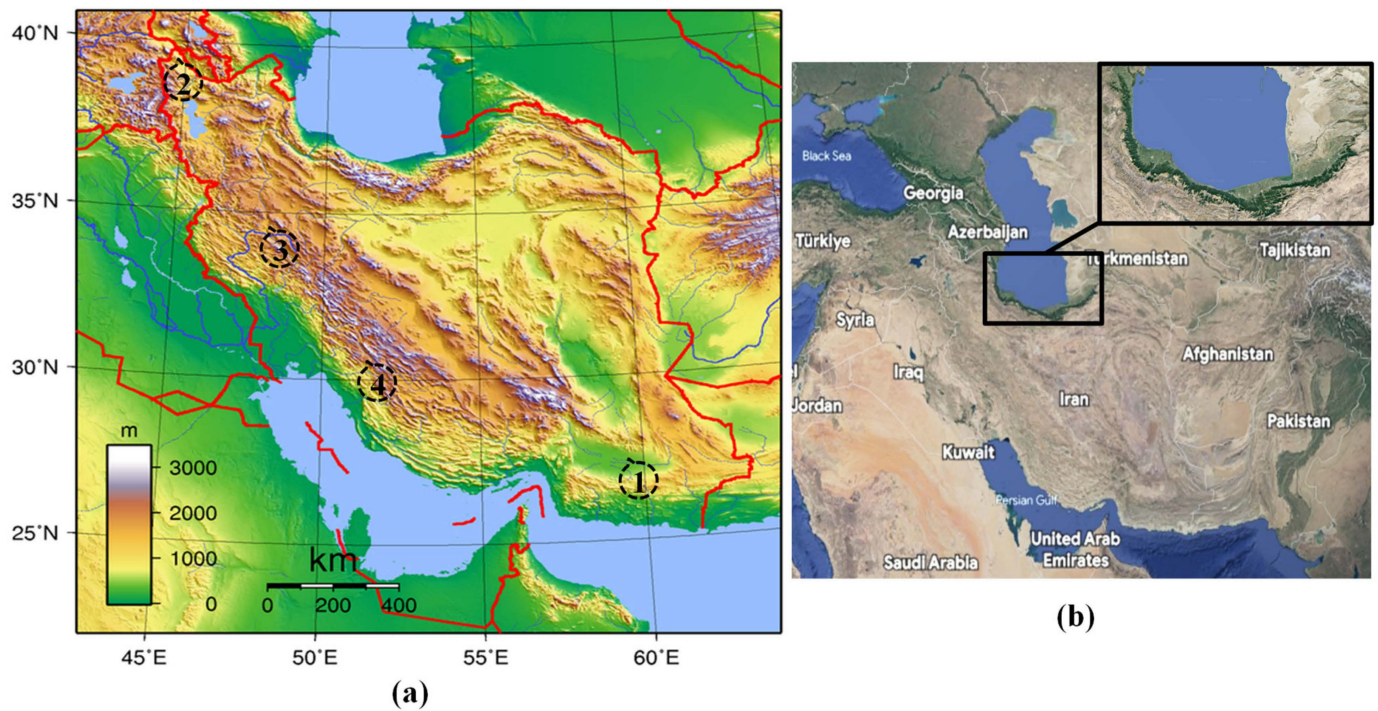


**Figure 2.** (a) Topographic map of Iran. (b) The location of the Hyrcanian forests in the north of Iran.

### 3. Aerodynamic Analysis

In the current research, the BEM model [65] was employed for computing the  $C_p$ . To do so, the blade was segmented into multiple distinct regions (elements), which exhibit aerodynamic behaviors similar to two-dimensional airfoils. Then, the aerodynamic forces were computed according to the local flow circumstances [66].

For computing the  $C_p$  value, initially, the blade was segmented into multiple distinct regions. For this purpose, based on previous works in this field, 10–20 regions were selected for the blade so that the aerodynamic forces applied to each of these regions and the distribution of these forces could be computed. Subsequently, an iterative process was employed to compute the tangential force coefficient ( $C_{a'}$ ), the tip loss factor ( $F$ ), the axial ( $a$ ) and rotational induction coefficients ( $a'$ ), the inflow angle ( $\phi$ ), the axial force coefficient ( $C_a$ ), and the solidity rate ( $\sigma$ ). Following the computation of  $a'$  and  $a$ , the power ( $dp$ ), as well as tangential ( $dF_y$ ) and axial forces ( $dF_x$ ), were computed for the blade sections. After the integration of these derivatives for the entire blade, the values of  $P$ ,  $F_y$ , and  $F_x$  along the blade were acquired, respectively [65]. Figure 3 depicts an SWT with timber blades and also the velocities on a blade element positioned at a radial distance of  $r$  from the center of the rotation.

To compute the  $C_p$ , the following measures were implemented:

Initially, a value of 0 was applied to both  $a'$  and  $a$ , and the algorithm was initiated by computing the  $\alpha$  and the inflow angle:

$$\phi = \tan^{-1} \left( \frac{(1-a)V}{(1+a')r\omega} \right) \quad (4)$$

$$C_a = C_l \cos \phi + C_d \sin \phi \quad (5)$$

in which  $\omega$ ,  $r$ , and  $V$  represent the rotational velocity, radius, and wind speed, respectively.

The following equations were employed to compute the  $C_{a'}$  and  $C_a$ :

$$C_a = C_l \cos \phi + C_d \sin \phi \tag{6}$$

$$C_{a'} = C_l \sin \phi - C_d \cos \phi \tag{7}$$

Subsequently, the Prandtl model was utilized to compute the blade tip losses:

$$F = \frac{2}{\pi} \cos^{-1} \left[ \exp \left( -\frac{B(R-r)}{2(r-\sin \phi)} \right) \right] \tag{8}$$

where  $R$  and  $B$  indicate the blade length and number, respectively.

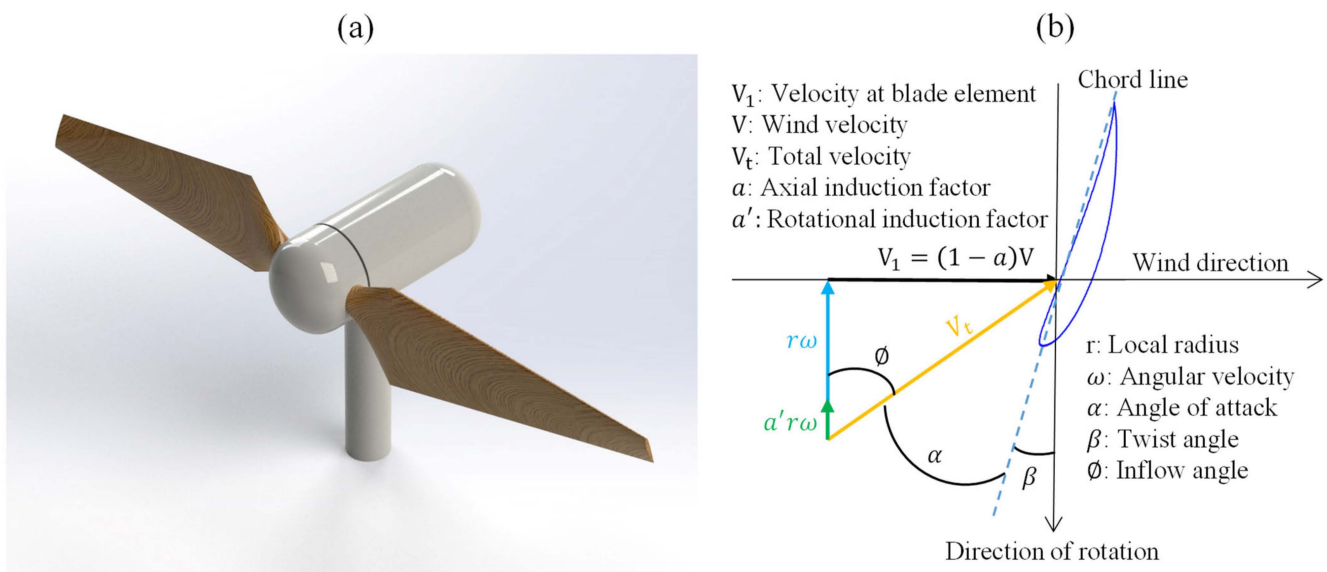


Figure 3. (a) A SWT with timber blades, and (b) the velocities of a blade element.

After that, the induction terms were calculated:

$$a = \frac{1}{\frac{4F \sin^2 \phi}{\sigma C_a} + 1} \tag{9}$$

$$a' = \frac{1}{\frac{4F \sin \phi \cos \phi}{\sigma C_{a'}} - 1} \tag{10}$$

where  $\sigma = \frac{Bc}{2\pi r}$  represents the solidity factor, in which  $c$  is the chord length.

At this stage, the computed induction terms were substituted in Equation (4), and the previous steps were repeated as long as these convergence criteria were not met:

$$|a_{n+1} - a_n| < 10^{-5} \tag{11}$$

$$|a'_{n+1} - a'_n| < 10^{-5} \tag{12}$$

After the determination of the induction term values,  $dF_y$ ,  $dF_x$ , and the total velocity ( $V_t$ ) could be computed using the following correlations:

$$V_t = \sqrt{[(1-a)V]^2 + [(1+a')r\omega]^2} \tag{13}$$

$$dF_x = \left( \frac{1}{2} \rho V_t^2 c dr \right) C_a \tag{14}$$

$$dF_y = \left( \frac{1}{2} \rho V_i^2 c dr \right) C_{a1} \quad (15)$$

in which  $\rho$  represents the air density.

Next, the power ( $dP$ ) and torque ( $dM$ ) for each blade section were computed from:

$$dM = r dF_y \quad (16)$$

$$dP = \omega dM \quad (17)$$

Considering  $B$ , the total power ( $P$ ) and aerodynamic moment ( $M$ ) were acquired:

$$M = B \sum_{i=1}^n (dM)_i \quad (18)$$

$$P = B \sum_{i=1}^n (dP)_i \quad (19)$$

In these correlations,  $n$  indicates the number of blade sections (elements).

The  $C_p$  value was then computed using:

$$C_p = \frac{M\omega}{0.5\rho S V^3} \quad (20)$$

where  $S$  represents the surface swept by the rotor.

Since the  $V$  value in the selected places was relatively low, to reduce the inertia and improve the startup behavior of the blades, the Bergéy BW-3 airfoil, which geometry is shown in Figure 4, was used as the blade profile. Having a high lift-to-drag ratio and possessing good aerodynamic performance in the presence of roughness were some features of this airfoil.

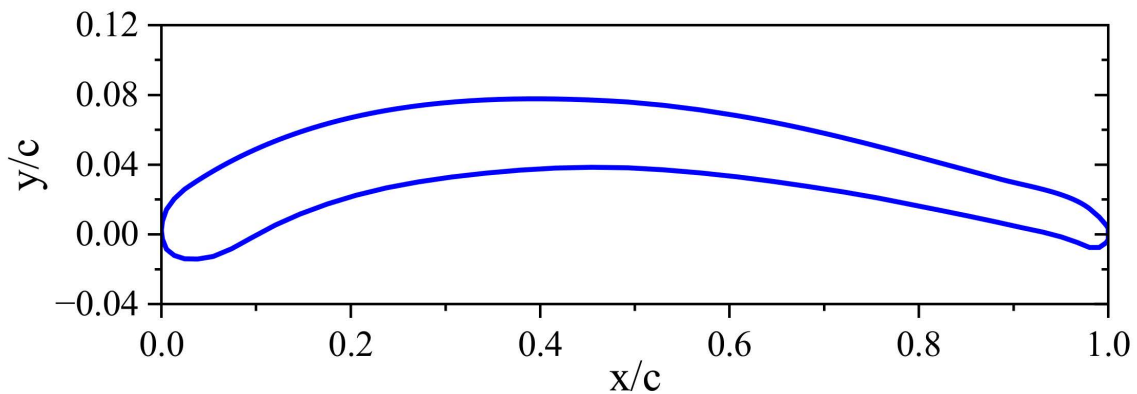


Figure 4. The Bergéy BW-3 airfoil profile.

Figure 5 shows the aerodynamic coefficients extracted from the experimental data conducted with the Bergéy BW-3 airfoil. In the current research, these coefficients were tabulated and coded, so that the corresponding aerodynamic coefficient was calculated and called during the computations considering the  $Re$  and the  $AOA$  of every individual element.

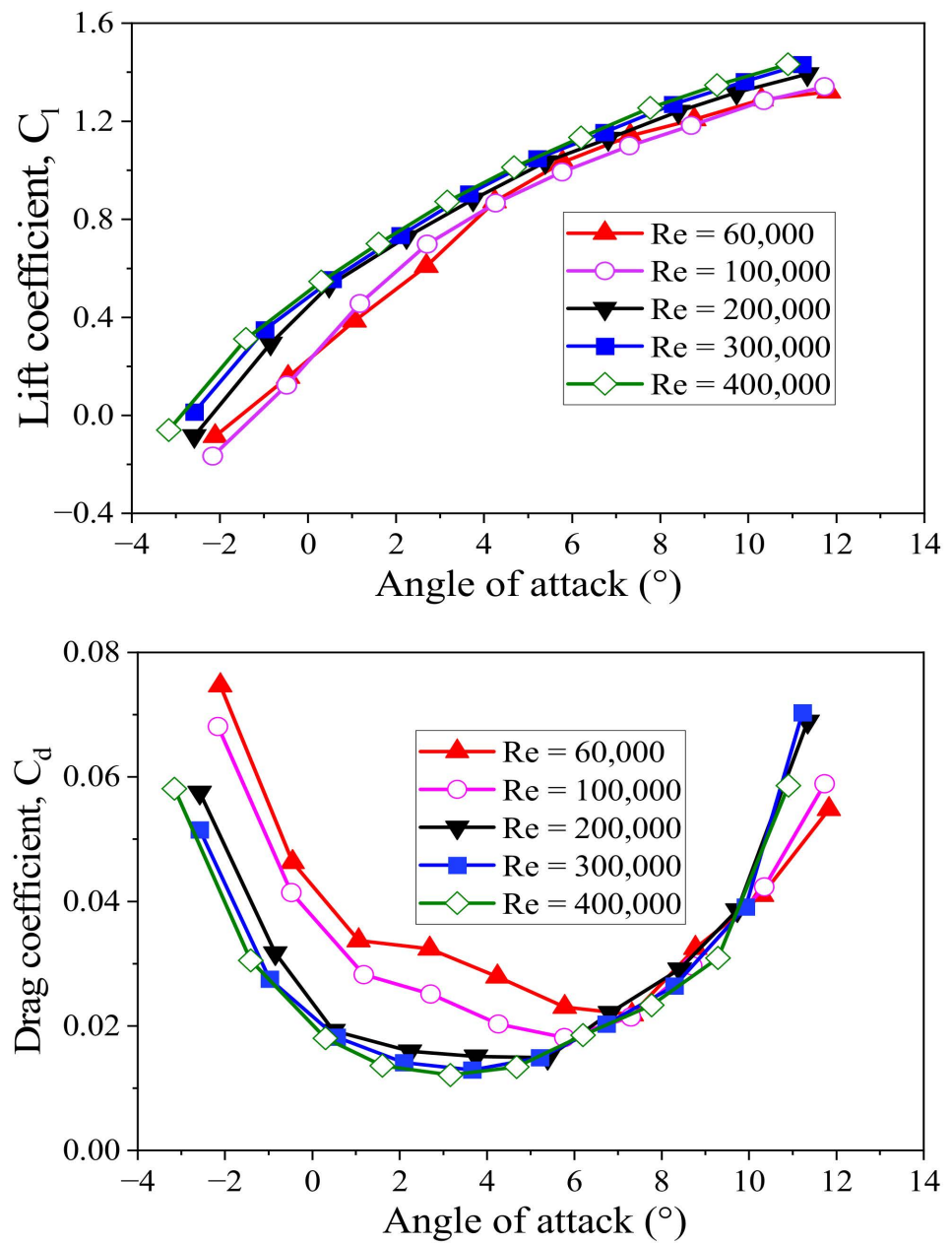


Figure 5. The lift and drag coefficients of the Bergye BW-3 airfoil at different  $Re$  and AOAs [67].

#### 4. Analyzing the Startup Time

When the turbine blades start to rotate, the AOA is high. Studies show that, at high AOAs, the aerodynamic behavior of airfoils is analogous to a flat plate. In this regard, Wood [9] presented the following correlation to calculate the startup torque ( $M_s$ ) generated by the blade during the startup process:

$$M_s = B\rho V^2 R^3 \int_{r_h}^1 (1 + \lambda_r^2)^{1/2} c r \sin \beta (\cos \beta - \lambda_r \sin \beta) dr \tag{21}$$

In this equation,  $r_h$  is the hub radius. It is also worth noting that all speeds and lengths in this equation have been nondimensionalized by  $V$  and  $R$ , respectively. The important point in Equation (21) is the independence of the  $M_s$  from the  $Re$ , which is due to using generic flat plate expressions to determine the aerodynamic coefficients at high AOAs. Also,  $c$  and  $r$  represent the chord length and the radial coordinate along the blade, respectively.

During the startup process of the blade from a static condition, the changes in the tip speed ratio ( $\lambda$ ) with time can be written as follows:

$$\frac{d\lambda}{dt} = \frac{R(M_s - M_c)}{JV} \quad (22)$$

where  $J$  is the blade inertia [9]:

$$J = B\rho_b AR^5 \left[ \int (c r)^2 dr + \frac{1}{12} \left( \int c^4 \cos^2 \beta dr + A^2 \int c^4 \sin^2 \beta dr \right) \right] \quad (23)$$

In this correlation,  $\rho_b$  is the blade density, and  $A$  is the area of the airfoil by assuming  $c = 1$ . Solving the differential Equation (22) from the static condition  $\lambda = 0$  to  $\lambda = 1$  determines the turbine startup time. Experimental studies have affirmed the reliability of Equation (22), and this correlation has been used by many researchers for computing the startup time of SWTs [9,21].

### 5. Multi-Objective Optimization and Input Parameters

The absence of any constraints such as continuity and derivability for the objective function, as well as demonstrating its effectiveness in solving multi-objective optimization problems, are two prominent characteristics of the DE algorithm, which was established by Storn and Price [68] in 1997. For this algorithm, there is no limit to the number of variables in the objective function, and this method only needs the objective function for execution, and its complexity does not impede the process. To find the optimal solution, three operators, including mutation, crossover, and selection, are used in the DE algorithm. In this technique, first, a random initial population (which is the blades in this study) is created based on the constraints considered for the design variables ( $\beta$  and  $c$  for this research); then, with the aid of the mutation and crossover operators, offsprings (new blades) are produced, and each child is compared against its parent with the aid of the selection operator. In case the child has a better objective value, it substitutes its parent, and the next generation is created. This process continues until reaching a global solution. In this regard, the steps taken in the DE algorithm in this study are briefly described as follows:

1. Initialization of the population and selecting the algorithm settings, including evolution administration and termination criterion.
2. Arbitrarily generating the population and computing objective function value for each member of the population.
3. Continuing these substeps unless the termination criteria are reached:
  - 3.1 Mutating with the difference vectors ( $x_{r1.g}$ ,  $x_{r2.g}$ , and  $x_{r3.g}$ ) according to the mutation factor ( $F$ ) and generating another vector ( $V_G = x_{r1.g} + F(x_{r2.g} - x_{r3.g})$ ).
  - 3.2 Crossing over based on the crossover constant ( $C_r$ ).
  - 3.3 Computing the objective function for the members of the population after the evolution.
  - 3.4 Selecting the optimal members based on the greatest value of the objective function.
4. Returning to the third step.

The two design goals considered in the present study, i.e., the  $C_p$  and startup time, are different. While the  $C_p$  has a numerical value of less than one, the startup time can possess any value. Thus, by nondimensionalizing and using the weighting coefficients method, which is one of the techniques for determining the Pareto front, the following objective function was considered for the optimization process, so that the DE algorithm tried to maximize this function [16]:

$$\text{Maximize} \left( W_f \frac{C_p}{\max(C_p)} + (1 - W_f) \frac{\min(T_s)}{T_s} \right) \quad (24)$$

where  $0 \leq W_f \leq 1$  is the weighting ratio that specifies the contribution of each of the design goals. Moreover,  $C_p$  is the power coefficient corresponding to the blades in the population matrix, and  $\max(C_p)$  is the highest power coefficient in each generation. On the other hand,  $T_s$  is the startup time corresponding to the blades in the population matrix, and  $\min(T_s)$  is the minimum startup time in each generation. With the aid of this objective function, the  $C_p$  and startup time in each generation are nondimensionalized, and the value of the objective function is between zero and one. The objective function constants,  $\max(C_p)$  and  $\min(T_s)$ , are variable during the execution of the algorithm, and therefore, the objective function also changes. The input parameters of the DE algorithm are given in Table 2. It is necessary to explain that, in the present study, a numerical code written using MATLAB R2014a software was used for the optimization.

**Table 2.** The values chosen for the DE algorithm variables.

Parameter	Population	Generation	Mutation Factor	Crossover Constant
Value	3000	500	0.8	0.1

The geometry of the WT blade is determined by three parameters, including the airfoil type and the  $\beta$  and  $c$  distributions. By choosing the Bergey BW-3 airfoil as the blade profile, the objective function variables are the  $\beta$  and the  $c$ . In the BEM theory, it is suggested to use between 10 and 20 elements along the blade [9]. In the present study, 15 elements were considered, and with this selection, the problem had 30 variables. Table 3 shows the input parameters and their values, along with the range of the design variables.

**Table 3.** Input values for design and optimization.

Parameter	Value	Parameter	Value	Parameter	Value
Output Power	1000 W	$V_s$	4 m/s	$R_H$	0.125 m
$B$	2	$V_{rated}$	8 m/s	$\omega$	450 rpm
Min $c/R$	0.01	Max $c/R$	0.2	$M_c$	0.5 Nm
Min $\beta$	-5	Max $\beta$	25	Generator inertia	0.01 kg·m <sup>2</sup>

The range considered for the  $c$  parameter is determined by the requirements of the manufacturing and machining process. To avoid excessive alternations while connecting the aerodynamic part of the blade to the root section, a maximum value of  $25^\circ$  was considered for the twist angle. Also, machining restrictions recommend a value of  $-5^\circ$  for the minimum twist angle. The considered  $M_c$  values, as well as its inertia, are among the characteristics of the selected one-kilowatt generator [44]. Since the selected countries do not have a significant wind potential [69], the startup wind speed ( $V_s$ ) of the turbine was selected to be 4 m/s. On the other hand, it is suggested that the rated speed in the design should not be less than twice the  $V_s$  value [9]. Thus, the design wind speed was chosen to be 8 m/s. The multi-objective optimization algorithm used in the present study is shown in Figure 6 in the form of a flowchart.

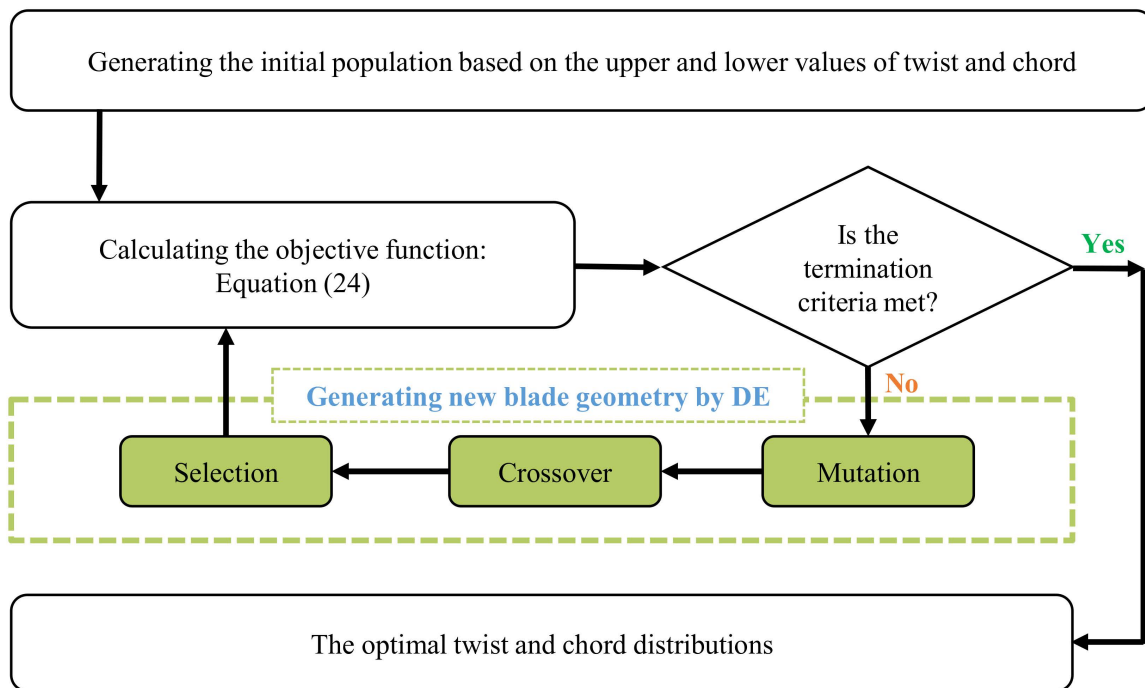


Figure 6. The optimization algorithm used in this research.

6. Validation

In this part, the accuracy of the developed in-house code is assessed. In this regard, in the first section, the  $C_p$  results, and in the second part, the startup time ( $T_s$ ) values, are validated.

6.1. Validation of the  $C_p$

In this section, the results of the current code are compared with the experimental data presented in Reference [70]. In this reference, the experimental data of a small two-blade WT with the NACA4412 airfoil as the blade profile and a rotor diameter of 3 m were presented at  $V = 10$  m/s. The aerodynamic coefficients of the related airfoil at diverse  $Re$  and  $AOAs$  [9] were tabulated, coded, and used in the relevant computations. The  $C_p$  values calculated from the numerical code have been compared against the experimental values in Figure 7. It can be perceived that the numerical results are in agreement with the reference data, having a maximum deviation of less than 6.5%.

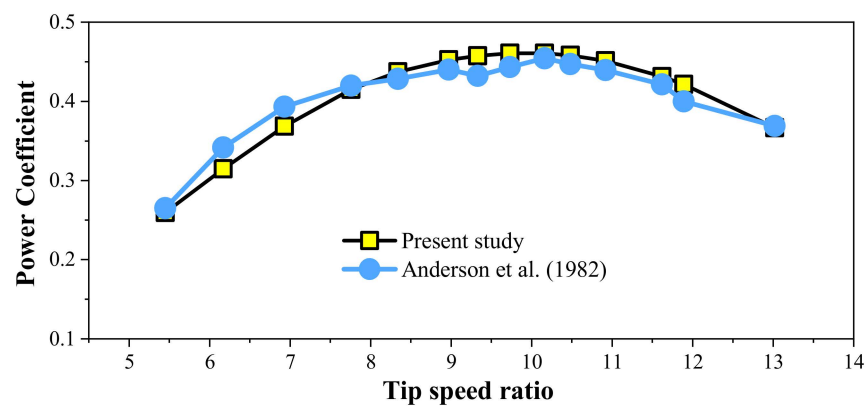


Figure 7. Comparing the values from the numerical code and Reference [70] data.

## 6.2. Validation of the $T_s$

To ensure that the startup results of the present code are valid, the numerical results of a small three-blade WT presented in Reference [16] were used. Considering the  $c$  and  $\beta$  values presented in this reference for ash blades with a density of  $590 \text{ kg/m}^3$ , the  $T_s$  was calculated. It is necessary to explain that, in Reference [16], the  $V_s$  was considered to be  $5 \text{ m/s}$ , and the SG6043 airfoil was used as the blade profile. Table 4 compares the  $T_s$  results. It is conspicuous that the results are significantly close to an absolute error of less than 2%.

**Table 4.** Comparison of the  $T_s$  from the developed code and Reference [16].

Parameter	Reference [16]	Current Research	Deviation (%)
Startup time (s)	5.1	5.2	1.96

## 7. Results and Discussion

In this section, two optimization processes are followed. In the first part, an SWT is designed for the elevation of the sea level; then, the influence of the selected timbers on its performance is evaluated, and the best blade is selected. Subsequently, the efficiency of the selected blade at various elevations is investigated. In the second part, to ameliorate the performance of the selected blade at each elevation, the blade is reconstructed. In this regard, the blade design will be based on the kinematic viscosity and air density of each region.

### 7.1. Designing a Blade for Operating at Sea Level and Evaluating Its Efficiency in the Selected Counties

According to Table 3, the generator considered in the current research generates  $1000 \text{ W}$  of power at a rated speed of  $450 \text{ rpm}$ , and its efficiency is  $75\%$  [44]. Therefore, by choosing a  $V$  of  $8 \text{ m/s}$ , which was explained in the previous section, the  $C_p$  and tip speed ratio of the turbine design can be acquired in terms of the blade length:

$$C_p = \frac{P/\eta}{0.5\rho SV^3} = \frac{1000/0.75}{0.5 \times 1.225 \times \pi R^2 \times 8^3} = \frac{1.35}{R^2} \quad (25)$$

$$\lambda = \frac{R\omega}{V} = \frac{450 \times 2\pi}{8 \times 60} R = 5.89R \quad (26)$$

By choosing any value for  $R$ , the corresponding values for  $C_p$  and  $\lambda$  are acquired. However, it should be noted that the value of  $C_p$  cannot exceed the Betz–Joukowsky limit ( $\frac{16}{27}$ ). The achievable  $C_p$  value in SWTs is reported to be  $0.48$  [9]. Considering this value for the  $C_p$ , the corresponding  $\lambda$  and  $R$  values are found to be  $9.9$  and  $1.68 \text{ m}$ , respectively (Figure 8). As was stated before, for the current research, a two-bladed turbine was chosen, the reasons for which are presented as follows:

1. In the design and optimization of wind turbines, it is necessary to select the number of blades based on the rated tip speed ratio ( $\lambda$ ). As explained by Manwell et al. [71] for the rated  $\lambda$  values higher than  $4$ , one to three blades offer the best performance for a wind turbine. Considering that, in the current work, the rate  $\lambda$  is  $9.9$ , the number of blades should be between one and three.

2. Changes in the power coefficient at various tip speed ratios in wind turbines with different numbers of blades show that, at high tip speed ratios, selecting more than two blades does not lead to a significant effect on the turbine power coefficient [71].

3. As discussed in the work of Tang et al. [72], the manufacturing cost of wind turbine blades accounts for around  $15$  to  $20\%$  of the total cost of the turbine. Therefore, to reduce manufacturing and maintenance costs as much as possible, the selection of a turbine with fewer blades seems reasonable.

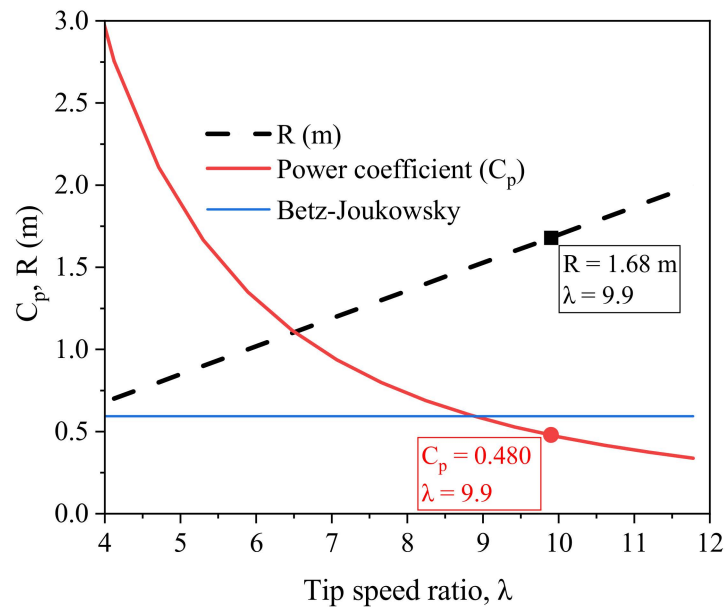


Figure 8. Variations in the blade length and the  $C_p$  at various tip speed ratios.

According to these points, it can be concluded that a two-bladed turbine is ideal for the present study. Now, it is possible to conduct the optimization process with the aid of the other input parameters (Tables 2 and 3).

The optimum values of the  $\beta$  and the  $c$  are provided in Figure 9 for the blade made of alder timber. Also, Table 5 summarizes the values of the  $C_p$  and optimal  $T_s$  for each of the selected timbers.

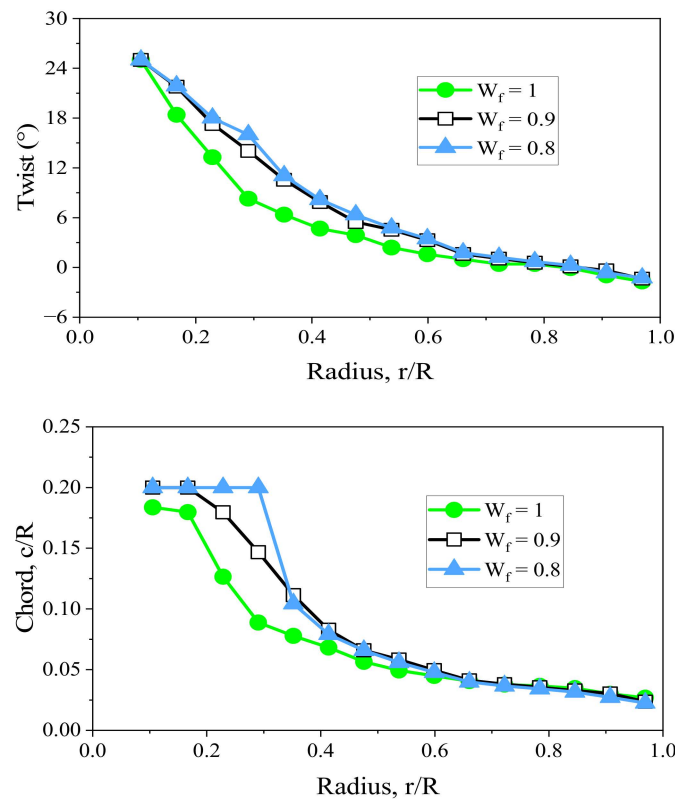
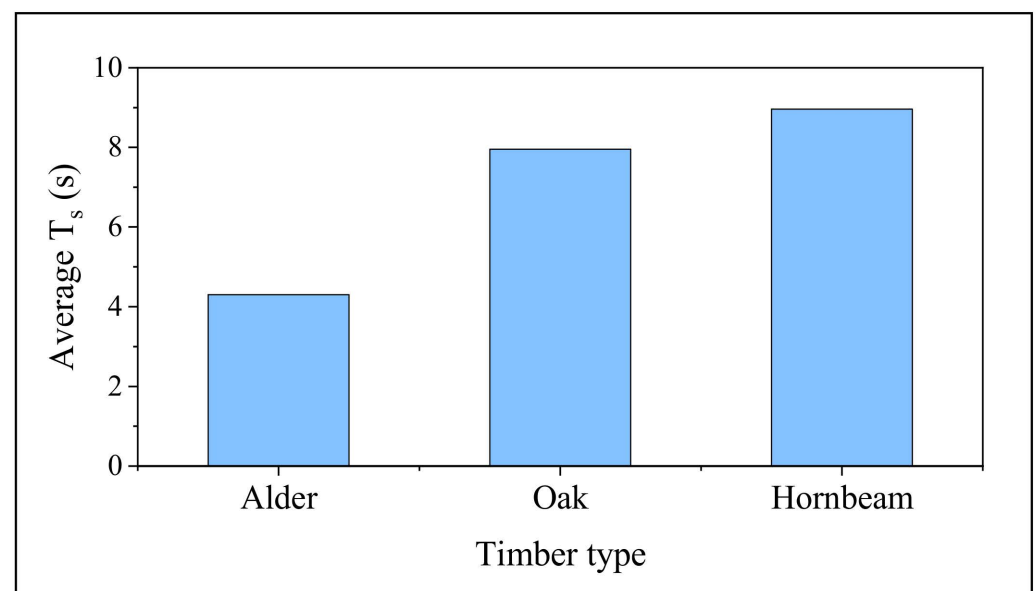


Figure 9. Optimum values of the  $\beta$  and the  $c$  of the blades made of Alder wood.

**Table 5.** The optimal  $C_p$  and  $T_s$  values for the blades made of each selected hardwood.

Timber	$\rho_b$ (kg/m <sup>3</sup> )	$W_f = 1$		$W_f = 0.9$		$W_f = 0.8$	
		$C_p$	$T_s$ (s)	$C_p$	$T_s$ (s)	$C_p$	$T_s$ (s)
Alder	490	0.480	8.08	0.469	2.75	0.446	2.12
Oak	600	0.479	17.86	0.469	3.39	0.444	2.61
Hornbeam	707	0.480	19.83	0.469	3.98	0.445	3.09

The density of these timbers is also given in this table. As can be observed, by diminishing the values of  $W_f$  in the objective function (Equation (24)), both the  $C_p$  and the  $T_s$  are decreased, but the reduction of the  $T_s$  is more considerable than the decrement in the  $C_p$ , so that, for the blade made of alder timber, by reducing the  $C_p$  by 7%, a 74% enhancement in the  $T_s$  is observed. The improvement of the  $T_s$  for the blades designed to be made of oak and hornbeam timbers is around 85%. This point underlines the significance of considering the  $T_s$  in the design of SWT blades, which do not possess a pitch control mechanism. According to Table 5, even though the blade density does not influence the turbine  $C_p$ , it substantially affects the  $T_s$ . Figure 10 depicts the average  $T_s$  of the optimal blades made of the selected timbers.

**Figure 10.** The average  $T_s$  for the optimal blades made from the selected timbers.

As can be observed, the time for the blades made of oak and hornbeam timbers is 84 and 108% more than the blades designed with alder wood, respectively. The reason for this is the low density of alder and, consequently, the lower inertia of the blades designed using this timber (Figure 11).

It is necessary to explain, besides the  $M_c$ , the  $M_s$  and the blade inertia are two factors that affect the startup behavior of SWTs. Based on Figure 9, as the value of  $W_f$  is reduced, the  $\beta$  and  $c$  values increase in the root elements. Raising the  $\beta$  values reduces the AOA of the root elements and increases the lift coefficient. On the other hand, based on Equation (21), the increment of the  $c$  also raises the  $M_s$ . In this regard, Figure 12 demonstrates that, for the blades made of alder timber, by reducing the value of  $W_f$ , the  $M_s$  increases.

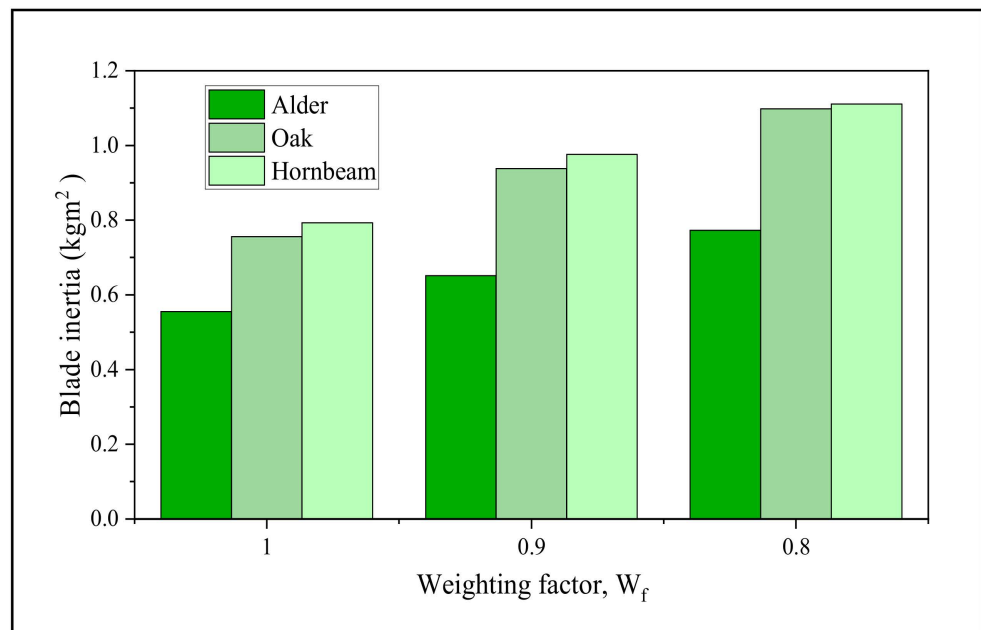


**Figure 11.** The inertia values for the blades made of the selected timbers with different  $W_f$  values.

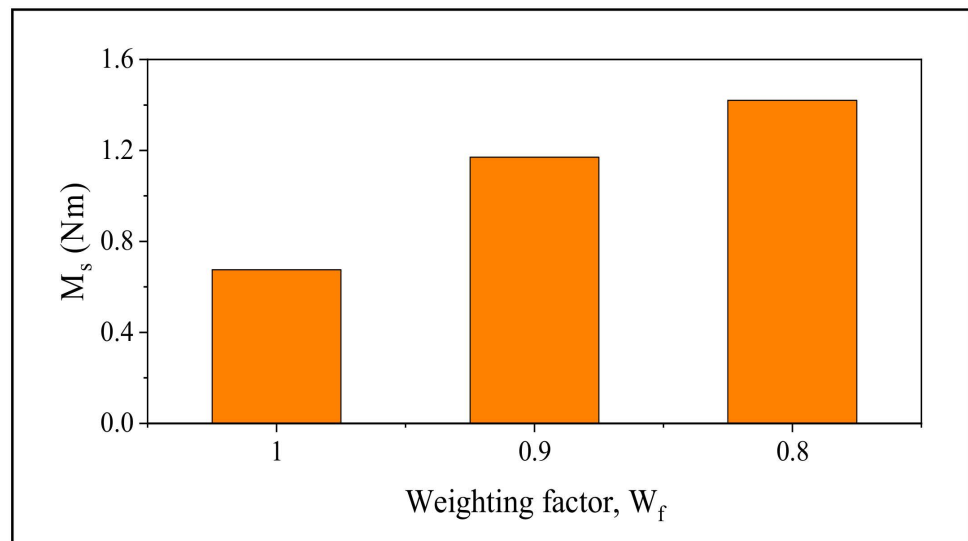


**Figure 12.** Increasing the  $M_s$  of the blades made of alder timber by reducing the value of  $W_f$ .

Regarding the increase in the  $c$ , it is essential to mention that, although raising this parameter causes an increase in the  $M_s$ , it also increases the blade inertia, which can hurt the turbine  $T_s$ ; thus, there is a conflict between the inertia and the  $M_s$ , for which the optimization algorithm tries to come up with a compromise by determining the optimal value for the  $c$ .

According to Table 5, the optimal blades made from alder timber have better performance than those made of the other selected timbers. Therefore, the aerodynamic behavior of these blades (designed with different  $W_f$  values) was investigated in the selected cities (Table 1), and the results are tabulated in Table 6.

**Table 6.** The performance of the optimal blades for the sea level (made of alder timber) at different elevations.

Case Study	$W_f = 1$		$W_f = 0.9$		$W_f = 0.8$	
	$C_p$	$T_s$ (s)	$C_p$	$T_s$ (s)	$C_p$	$T_s$ (s)
Dalgan (392 m)	0.477	20.71	0.466	2.95	0.443	2.26
Maku (1182 m)	0.475	61.67	0.462	3.42	0.441	2.58
Asadabad (1607 m)	0.471	-	0.460	3.72	0.439	2.77
Sisakht (2250 m)	0.470	-	0.457	4.26	0.436	3.11

It can be perceived that, as the elevation increases, the  $C_p$  is reduced while the  $T_s$  rises. Even though the decrease in the  $C_p$  due to the reduction in the  $Re$  (because of the increase in kinematic viscosity) can be up to 2.5%, the increase in the  $T_s$  is notable, so that the ideal blade ( $W_f = 1$ ), which was designed to work at the sea level, cannot start to spin at  $V = 4$  m/s in the cities of Asadabad and Sisakht, and it practically loses its performance. In these regions, the generated  $M_s$  cannot conquer the  $M_c$ , which has a meaningful value in SWTs (as compared to the  $M_s$  generated in these turbines). This point affirms that, in the design and selection of SWT blades, the parameter of elevations above sea level should be considered.

### 7.2. Redesigning the Blades for Each County

In this section, the blades are redesigned for each elevation based on the standard air conditions presented in Table 1, and the findings are given in Table 7.

It can be perceived that, by accounting for the effect of elevation in the design, the overall performance of the blades has improved compared to the results in Table 6, so that the redesigned ideal blades can start rotating and be employed to generate power in Asadabad and Sisakht Counties. To investigate the reason for this issue, the geometry of the optimized blade redesigned for the highest elevation, i.e., Sisakht County, along with the optimized blade geometry designed to work at sea level, are compared in Figure 13. It can be perceived that, while the  $\beta$  values are almost the same in both blades, the  $c$  of the blade redesigned to work at a higher elevation is generally greater than that of the blade designed to work at sea level. Indeed, with the rise in elevation (increase in the kinematic viscosity), the  $Re$  on the blade decreases, which will lead to a decrement in the lift coefficient of the blade. Therefore, the optimization algorithm tries to raise the lift coefficient and, as a result, the energy harnessed from the wind to improve the  $C_p$  and prevent its drastic reduction by raising the  $c$ . On the other hand, as mentioned before, the increase in the  $c$  also results in an increment in the  $M_s$ , which enables the blades to rotate at  $V = 4$  m/s.

**Table 7.** The performance of the optimal blades for the sea level (made of alder timber) at different elevations.

Case Study	$W_f = 1$		$W_f = 0.9$		$W_f = 0.8$	
	$C_p$	$T_s$ (s)	$C_p$	$T_s$ (s)	$C_p$	$T_s$ (s)
Dalgan (392 m)	0.479	6.73	0.468	2.95	0.446	2.28
Maku (1182 m)	0.479	9.35	0.467	3.39	0.444	2.58
Asadabad (1607 m)	0.479	11.89	0.466	3.67	0.444	2.78
Sisakht (2250 m)	0.478	17.76	0.465	4.22	0.442	3.27

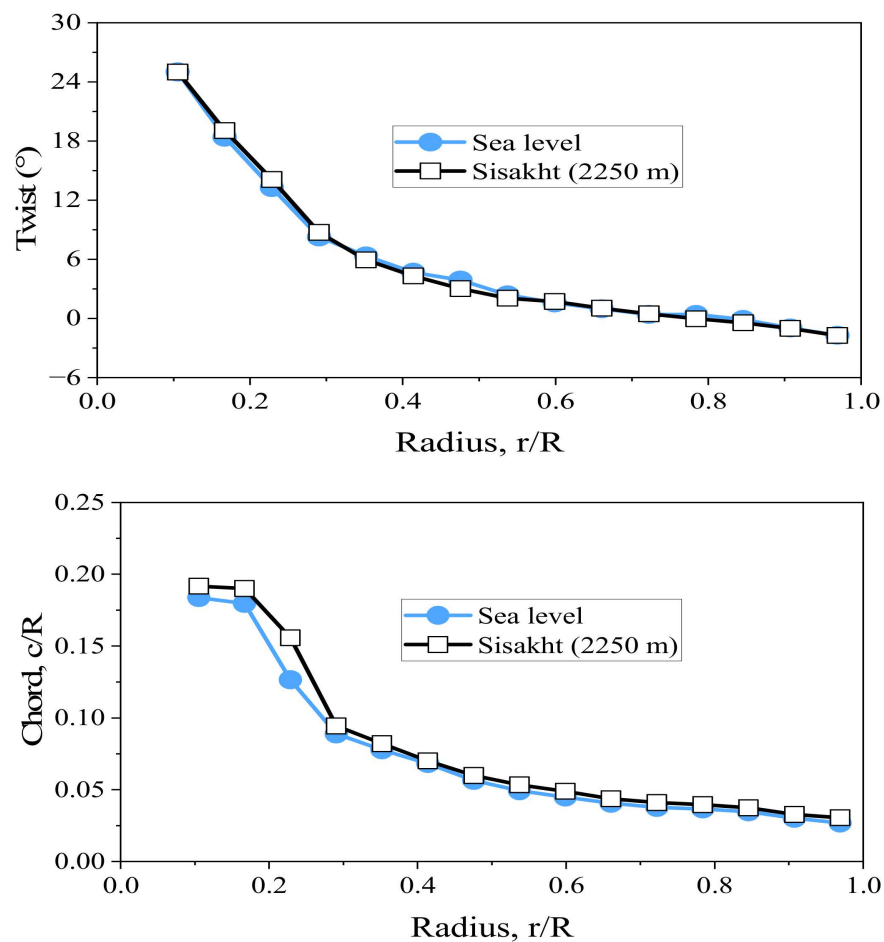


**Figure 13.** The geometric shape of the optimal blades at sea level and the elevation of 2250 m.

## 8. Conclusions

Wood is a stable, cheap, and durable engineering material that has good fatigue resistance. This material has been an interesting choice for application in SWT blades in recent years. Moreover, SWTs are installed in areas with different elevations. This study examines the impacts of wood density and elevations above sea level on the performance of a small 1-kW wind turbine. For this purpose, the usage of three hardwoods—namely, alder, oak, and hornbeam—which grow abundantly in the Hyrcanian forests of Iran as the materials of SWT blades and four low-wind counties, including Delgan, Maku, Asadabad, and Sisakht, with different elevations above sea level were selected as the case studies. To reduce the blade inertia, the Bergey BW-3 airfoil, which has a smaller area compared to other airfoils used in the SWT industry, was used as the blade profile. Additionally, to reduce the cost, a rotor with two blades was selected. Considering that the wind speed is not high in the selected counties, minimizing the startup time ( $T_s$ ) was added to the main design goal, which was maximizing the power coefficient ( $C_p$ ) of the turbine. Then, based on these objectives, the geometric shape of the blades was determined with the aid of the DE algorithm. The BEM model (along with the Prandtl model for accounting for the blade tip losses) was utilized to compute the  $C_p$ , and a quasi-steady version of the BEM model was employed to calculate the  $T_s$ . The findings showed that the hardwood type utilized in the blade has no impact on the  $C_p$ , but it utterly influences the  $T_s$ , so that the average  $T_s$  of the blades made of oak and hornbeam timbers are 84 and 108% higher than the average  $T_s$  of the optimized blades made of alder timber. It is highly recommended to consider the  $T_s$  for the design and optimization of wind turbine blades in less windy regions, because the results demonstrate that, with only about a 7% reduction in the  $C_p$ , the  $T_s$  of the blades made of alder improves by 74%, and the enhancement of the  $T_s$  for the

blades made of oak and hornbeam timbers is around 85%. This undeniable improvement stems from raising the twist angle and chord length in the root elements of the blades. In addition, it was observed that the performance of the turbine that was designed to work at sea level was weakened at greater elevations. Although the change in the  $C_p$  can be ignored, the startup performance is prone to more severe impacts, and the reduction in the startup torque ( $M_s$ ) can be so drastic that it practically stops the turbine from operating in these regions, since the rotor cannot conquer the generator cogging torque ( $M_c$ ) and start rotating. In this case, the turbine loses its performance and cannot be used to generate power. This phenomenon was observed for the two-bladed turbine of the current research in Asadabad and Sisakht Counties, with elevations of 1607 and 2250 m above sea level. To solve this problem, the blade was redesigned based on the local atmospheric conditions in which the turbine was intended to be used, and improvements were observed in the  $C_p$  and  $T_s$  of the blades, especially the ideal blades.

**Author Contributions:** Conceptualization, V.A.; methodology, V.A., M.N. and R.K.; software, V.A.; validation, V.A.; formal analysis, R.K.; investigation, V.A.; resources, W.Y.; data curation, V.A.; writing—original draft preparation, V.A.; writing—review and editing, W.Y.; visualization, V.A.; supervision, M.N., R.K. and W.Y.; project administration, M.N.; and funding acquisition, W.Y. All authors have read and agreed to the published version of the manuscript.

**Funding:** This research received no external funding.

**Institutional Review Board Statement:** Not applicable.

**Informed Consent Statement:** Not applicable.

**Data Availability Statement:** The data presented in this study are available on reasonable request from the corresponding author.

**Conflicts of Interest:** The authors declare no conflict of interest.

## References

- Ahmadi, M.H.; Hosseini Dehshiri, S.S.; Hosseini Dehshiri, S.J.; Mostafaeipour, A.; Almutairi, K.; Ao, H.X.; Rezaei, M.; Techato, K. A Thorough Economic Evaluation by Implementing Solar/Wind Energies for Hydrogen Production: A Case Study. *Sustainability* **2022**, *14*, 1177. [[CrossRef](#)]
- Pastromas, S.; Pyrgioti, E. Modular Lightning Protection for Wind Turbines. *Wind* **2023**, *3*, 115–130. [[CrossRef](#)]
- Belaïd, F.; Al-Sarihi, A.; Al-Mestneer, R. Balancing Climate Mitigation and Energy Security Goals amid Converging Global Energy Crises: The Role of Green Investments. *Renew. Energy* **2023**, *205*, 534–542. [[CrossRef](#)]
- Hosseini, S.E. Transition Away from Fossil Fuels toward Renewables: Lessons from Russia-Ukraine Crisis. *Future Energy* **2022**, *1*, 2–5. [[CrossRef](#)]
- Mostafaeipour, A.; Jahangiri, M.; Haghani, A.; Dehshiri, S.J.H.; Dehshiri, S.S.H.; Issakhov, A.; Sedaghat, A.; Saghaei, H.; Akinlabi, E.T.; Sichilalu, S.M.; et al. Statistical Evaluation of Using the New Generation of Wind Turbines in South Africa. *Energy Reports* **2020**, *6*, 2816–2827. [[CrossRef](#)]
- Refan, M.; Hangan, H. Aerodynamic Performance of a Small Horizontal Axis Wind Turbine. *J. Sol. Energy Eng.* **2012**, *134*, 021013. [[CrossRef](#)]
- Plaza, B.; Bardera, R.; Visiedo, S. Comparison of BEM and CFD Results for MEXICO Rotor Aerodynamics. *J. Wind Eng. Ind. Aerodyn.* **2015**, *145*, 115–122. [[CrossRef](#)]
- Sun, S.Y.; Liu, H.J.; Peng, H.Y. Power Performance and Self-Starting Features of H-Rotor and Helical Vertical Axis Wind Turbines with Different Airfoils in Turbulence. *Energy Convers. Manag.* **2023**, *292*, 117405. [[CrossRef](#)]
- Wood, D. Green energy and technology. In *Small Wind Turbines: Analysis, Design, and Application*; Springer: London, UK, 2011; Volume 38, ISBN 9781849961745.
- Riziotis, V.A.; Voutsinas, S.G. Fatigue Loads on Wind Turbines of Different Control Strategies Operating in Complex Terrain. *J. Wind Eng. Ind. Aerodyn.* **2000**, *85*, 211–240. [[CrossRef](#)]
- Corbus, D.; Prascher, D. Analysis and Comparison of Test Results from the Small Wind Research Turbine Test Project. In Proceedings of the 43rd AIAA Aerospace Sciences Meeting and Exhibit, Reno, NV, USA, 10–13 January 2005; p. 778.
- Ismail, A. Wind Turbine Blade Dynamics Simulation under the Effect of Atmospheric Turbulence. *Emerg. Sci. J.* **2023**, *7*, 162–176. [[CrossRef](#)]
- Nandi, T.N. *Effects of Blade Boundary Layer Transition and Daytime Atmospheric Turbulence on Wind Turbine Performance Analyzed with Blade-Resolved Simulation and Field Data*; The Pennsylvania State University: London, UK, 2017; ISBN 1369992076.

14. Churchfield, M.J.; Lee, S.; Michalakes, J.; Moriarty, P.J. A Numerical Study of the Effects of Atmospheric and Wake Turbulence on Wind Turbine Dynamics. *J. Turbul.* **2012**, *13*, N14. [[CrossRef](#)]
15. Nandi, T.N.; Herrig, A.; Brasseur, J.G. Non-Steady Wind Turbine Response to Daytime Atmospheric Turbulence. *Philos. Trans. R. Soc. A Math. Phys. Eng. Sci.* **2017**, *375*, 20160103. [[CrossRef](#)]
16. Pourrajabian, A.; Dehghan, M.; Javed, A.; Wood, D. Choosing an Appropriate Timber for a Small Wind Turbine Blade: A Comparative Study. *Renew. Sustain. Energy Rev.* **2019**, *100*, 1–8. [[CrossRef](#)]
17. Lubitz, W.D. Impact of Ambient Turbulence on Performance of a Small Wind Turbine. *Renew. Energy* **2014**, *61*, 69–73. [[CrossRef](#)]
18. Karthikeyan, N.; Kalidasa Murugavel, K.; Arun Kumar, S.; Rajakumar, S. Review of Aerodynamic Developments on Small Horizontal Axis Wind Turbine Blade. *Renew. Sustain. Energy Rev.* **2015**, *42*, 801–822. [[CrossRef](#)]
19. Vaz, J.R.P.; Wood, D.H.; Bhattacharjee, D.; Lins, E.F. Drivetrain Resistance and Starting Performance of a Small Wind Turbine. *Renew. Energy* **2018**, *117*, 509–519. [[CrossRef](#)]
20. Pourrajabian, A.; Rahgozar, S.; Dehghan, M.; Wood, D. A Comprehensive Multi-Objective Optimization Study for the Aerodynamic Noise Mitigation of a Small Wind Turbine. *Eng. Anal. Bound. Elem.* **2023**, *155*, 553–564. [[CrossRef](#)]
21. Rahgozar, S.; Pourrajabian, A.; Kazmi, S.A.A.; Kazmi, S.M.R. Performance Analysis of a Small Horizontal Axis Wind Turbine under the Use of Linear/Nonlinear Distributions for the Chord and Twist Angle. *Energy Sustain. Dev.* **2020**, *58*, 42–49. [[CrossRef](#)]
22. Liu, J.; Xiao, Z.; Fu, S. Unsteady Transition Studies over a Pitching Airfoil Using Ak- $\omega$ - $\gamma$  Transition Model. *AIAA J.* **2018**, *56*, 3776–3781. [[CrossRef](#)]
23. Nandi, T.N.; Brasseur, J.G.; Vijayakumar, G. *Prediction and Analysis of the Nonsteady Transition and Separation Processes on an Oscillating Wind Turbine Airfoil Using the  $\gamma$ -Re- $\theta$  Transition Model*; Penn State University: University Park, PA, USA, 2016.
24. Eltayesh, A.; Castellani, F.; Burlando, M.; Hanna, M.B.; Huzayyin, A.S.; El-Batsh, H.M.; Becchetti, M. Experimental and Numerical Investigation of the Effect of Blade Number on the Aerodynamic Performance of a Small-Scale Horizontal Axis Wind Turbine. *Alexandria Eng. J.* **2021**, *60*, 3931–3944. [[CrossRef](#)]
25. Astolfi, D.; Pandit, R.; Lombardi, A.; Terzi, L. Diagnosis of Wind Turbine Systematic Yaw Error through Nacelle Anemometer Measurement Analysis. *Sustain. Energy Grids Netw.* **2023**, *34*, 101071. [[CrossRef](#)]
26. *61400-2 IEC:2006; Wind Turbines—Part 2: Small Wind Turbines*. IEC: Geneva, Switzerland, 2013.
27. Zhang, Q.; Wang, X. Numerical Investigation of Aerodynamic Performances for NREL 5-MW Offshore Wind Turbine. *Wind* **2023**, *3*, 191–212. [[CrossRef](#)]
28. Castellani, F.; Astolfi, D.; Peppoloni, M.; Natili, F.; Buttà, D.; Hirschl, A. Experimental Vibration Analysis of a Small Scale Vertical Wind Energy System for Residential Use. *Machines* **2019**, *7*, 35. [[CrossRef](#)]
29. Sessarego, M.; Dixon, K.R.; Rival, D.E.; Wood, D.H. A Hybrid Multi-Objective Evolutionary Algorithm for Wind-Turbine Blade Optimization. *Eng. Optim.* **2015**, *47*, 1043–1062. [[CrossRef](#)]
30. Hsu, C.-H.; Chen, J.-L.; Yuan, S.-C.; Kung, K.-Y. CFD Simulations on the Rotor Dynamics of a Horizontal Axis Wind Turbine Activated from Stationary. *Appl. Mech.* **2021**, *2*, 147–158. [[CrossRef](#)]
31. Gasch, R.; Tvele, J. Blade Geometry According to Betz and Schmitz. In *Wind Power Plants: Fundamentals, Design, Construction and Operation*; Springer: New York, NY, USA, 2011; pp. 168–207.
32. Akbari, V.; Naghashadegan, M.; Kouhikamali, R.; Afsharpanah, F.; Yaïci, W. Multi-Objective Optimization of a Small Horizontal-Axis Wind Turbine Blade for Generating the Maximum Startup Torque at Low Wind Speeds. *Machines* **2022**, *10*, 785. [[CrossRef](#)]
33. Burton, T.; Jenkins, N.; Sharpe, D.; Bossanyi, E. *Wind Energy Handbook*; John Wiley & Sons: New York, NY, USA, 2011; ISBN 111999392X.
34. Akbari, V.; Naghashadegan, M.; Kouhikamali, R.; Afsharpanah, F.; Yaïci, W. Multi-Objective Optimization and Optimal Airfoil Blade Selection for a Small Horizontal-Axis Wind Turbine (HAWT) for Application in Regions with Various Wind Potential. *Machines* **2022**, *10*, 687. [[CrossRef](#)]
35. Cheraghalipour, A.; Hajiaghaei-Keshteli, M.; Paydar, M.M. Tree Growth Algorithm (TGA): A Novel Approach for Solving Optimization Problems. *Eng. Appl. Artif. Intell.* **2018**, *72*, 393–414. [[CrossRef](#)]
36. El Sheshtawy, H.; el Moctar, O.; Natarajan, S. Multi-Point Shape Optimization of a Horizontal Axis Tidal Stream Turbine. *Eng* **2021**, *2*, 340–355. [[CrossRef](#)]
37. Shinde, P.; Ohol, S.S.; Tripathi, V.K. Shape Optimization of an Asymmetric Airfoil for Low Wind Speed Region Having Adjoint-Based Optimization Technique. *J. Appl. Fluid Mech.* **2023**, *16*, 299–310. [[CrossRef](#)]
38. Schröder, K.; Gebhardt, C.; Rolfes, R. Damage Localization at Wind Turbine Support Structures Using Sequential Quadratic Programming for Model Updating. In *Proceedings of the 8th European Workshop On Structural Health Monitoring, Bilbao, Spain, 5–8 July 2016*.
39. Ashuri, T.; Zaaijer, M.B.; Martins, J.R.R.A.; Van Bussel, G.J.W.; Van Kuik, G.A.M. Multidisciplinary Design Optimization of Offshore Wind Turbines for Minimum Levelized Cost of Energy. *Renew. Energy* **2014**, *68*, 893–905. [[CrossRef](#)]
40. Vieira, J.C.; Vieira, A.C.; Ribeiro, M.L.; Fiadeiro, P.T.; Costa, A.P. Angle of the Perforation Line to Optimize Partitioning Efficiency on Toilet Papers. *Eng* **2023**, *4*, 80–91. [[CrossRef](#)]
41. Biswas, P.P.; Suganthan, P.N.; Amaratunga, G.A.J. Optimization of Wind Turbine Rotor Diameters and Hub Heights in a Windfarm Using Differential Evolution Algorithm. In *Proceedings of the Sixth International Conference on Soft Computing for Problem Solving: SocProS 2016, Patiala, India, 23–24 December 2016*; Springer: New York, NY, USA, 2017; Volume 2, pp. 131–141.

42. Merzoug, A.; Rasouli, V. Offset Well Design Optimization Using a Surrogate Model and Metaheuristic Algorithms: A Bakken Case Study. *Eng* **2023**, *4*, 1290–1305. [[CrossRef](#)]
43. Ahmad, M.F.; Isa, N.A.M.; Lim, W.H.; Ang, K.M. Differential Evolution: A Recent Review Based on State-of-the-Art Works. *Alexandria Eng. J.* **2022**, *61*, 3831–3872. [[CrossRef](#)]
44. Pourrajabian, A.; Ebrahimi, R.; Mirzaei, M. Applying Micro Scales of Horizontal Axis Wind Turbines for Operation in Low Wind Speed Regions. *Energy Convers. Manag.* **2014**, *87*, 119. [[CrossRef](#)]
45. Abdelsalam, A.M.; El-Askary, W.A.; Kotb, M.A.; Sakr, I.M. Experimental Study on Small Scale Horizontal Axis Wind Turbine of Analytically-Optimized Blade with Linearized Chord Twist Angle Profile. *Energy* **2021**, *216*, 119304. [[CrossRef](#)]
46. Clausen, P.D.; Evans, S.P.; Wood, D.H. 13—Design, Manufacture, and Testing of Small Wind Turbine Blades. In *Woodhead Publishing Series in Energy*; Brøndsted, P., Nijssen, R., Goutianos, S.B.T.-A., Eds.; Woodhead Publishing: Cambridge, UK, 2023; pp. 441–461, ISBN 978-0-08-103007-3.
47. Peterson, P.; Clausen, P.D. Timber for High Efficiency Small Wind Turbine Blades. *Wind Eng.* **2004**, *28*, 87. [[CrossRef](#)]
48. Astle, C.; Burge, I.; Chen, M.; Herrler, T.; Kwan, L.; Zibin, N.; Wood, D. Timber for Small Wind Turbine Blades. *Energy Sustain. Dev.* **2013**, *17*, 671–676. [[CrossRef](#)]
49. Clausen, P.; Whale, J.; Wood, D. *Small Wind and Hydrokinetic Turbines*; IET: London, UK, 2021; Volume 169, ISBN 1839530715.
50. Friedrich, K.; Lukas, M. *History of Wind Energy and an Outlook for the Future BT—Towards 100% Renewable Energy*; Uyar, T.S., Ed.; Springer International Publishing: Cham, Switzerland, 2017; pp. 401–418.
51. Energy, R. Energy Efficiency Organization (SATBA), Iran. Available online: [www.sabta.gov.ir](http://www.sabta.gov.ir) (accessed on 8 June 2023).
52. Mirnezami, S.R.; Mohseni Cheraghloou, A. Wind Power in Iran: Technical, Policy, and Financial Aspects for Better Energy Resource Management. *Energies* **2022**, *15*, 3230. [[CrossRef](#)]
53. Jung, C.; Schindler, D. Efficiency and Effectiveness of Global Onshore Wind Energy Utilization. *Energy Convers. Manag.* **2023**, *280*, 116788. [[CrossRef](#)]
54. Dabbaghian, A.; Fazelpour, F.; Abnavi, M.D.; Rosen, M.A. Evaluation of Wind Energy Potential in Province of Bushehr, Iran. *Renew. Sustain. Energy Rev.* **2016**, *55*, 455–466. [[CrossRef](#)]
55. Mostafaeipour, A.; Jadidi, M.; Mohammadi, K.; Sedaghat, A. An Analysis of Wind Energy Potential and Economic Evaluation in Zahedan, Iran. *Renew. Sustain. Energy Rev.* **2014**, *30*, 641–650. [[CrossRef](#)]
56. Fazelpour, F.; Soltani, N.; Soltani, S.; Rosen, M.A. Assessment of Wind Energy Potential and Economics in the North-Western Iranian Cities of Tabriz and Ardabil. *Renew. Sustain. Energy Rev.* **2015**, *45*, 87–99. [[CrossRef](#)]
57. Keyhani, A.; Ghasemi-Varnamkhasti, M.; Khanali, M.; Abbaszadeh, R. An Assessment of Wind Energy Potential as a Power Generation Source in the Capital of Iran, Tehran. *Energy* **2010**, *35*, 188–201. [[CrossRef](#)]
58. Mohammadi, S.; Maleki, A.; Ehsani, R.; Shakouri, O. Investigation of Wind Energy Potential in Zanjan Province, Iran. *Renew. Energy Res. Appl.* **2022**, *3*, 61–70.
59. Nedaei, M. Wind energy potential assessment in Chalus County in Iran. *Int. J. Renew. Energy Res.* **2012**, *2*, 338–347.
60. Mirhosseini, M.; Sharifi, F.; Sedaghat, A. Assessing the Wind Energy Potential Locations in Province of Semnan in Iran. *Renew. Sustain. Energy Rev.* **2011**, *15*, 449–459. [[CrossRef](#)]
61. Mostafaeipour, A. Feasibility Study of Offshore Wind Turbine Installation in Iran Compared with the World. *Renew. Sustain. Energy Rev.* **2010**, *14*, 1722–1743. [[CrossRef](#)]
62. United States Committee on Extension to the Standard Atmosphere, United States; Air Force, United States; Weather Bureau, United States. *US Standard Atmosphere*; National Oceanic and Atmospheric Administration, National Aeronautics: Washington, DC, USA, 1962.
63. Adeli, K.; Yachkaschi, A.; Mohammadi Limaiei, S.; Fallah, A. A Study of the Condition of Timber Production in Iran and the Expected Production Rate in the next Decade. *J. Sustain. Dev.* **2012**, *5*, 144–154. [[CrossRef](#)]
64. Kiaei, M.; Samariha, A. Fiber Dimensions, Physical and Mechanical Properties of Five Important Hardwood Plants. *Indian J. Sci. Technol.* **2011**, *4*, 1460–1463. [[CrossRef](#)]
65. Gundtoft, S. Wind Turbines. *Univ. Coll. Aarhus* **2009**, 7–8. Available online: [https://scholar.google.com/scholar\\_lookup?title=Wind+Turbines&author=Gundtoft,+S.&publication\\_year=2009](https://scholar.google.com/scholar_lookup?title=Wind+Turbines&author=Gundtoft,+S.&publication_year=2009) (accessed on 8 June 2023).
66. Spyropoulos, N.; Papadakis, G.; Prospathopoulos, J.M.; Riziotis, V.A. Investigating the Level of Fidelity of an Actuator Line Model in Predicting Loads and Deflections of Rotating Blades under Uniform Free-Stream Flow. *Appl. Sci.* **2021**, *11*, 12097. [[CrossRef](#)]
67. Lyon, C.A.; Broeren, A.P.; Giguere, P.; Gopalarathnam, A.; Selig, M.S. *Summary of Low-Speed Airfoil Data*; Soartech: Virginia Beach, VA, USA, 1997; Volume 3, ISBN 0-9646747-3-4.
68. Storn, R.; Price, K. Differential Evolution—A Simple and Efficient Heuristic for Global Optimization over Continuous Spaces. *J. Glob. Optim.* **1997**, *11*, 341–359. [[CrossRef](#)]
69. Razeghi, M.; Hajinezhad, A.; Naseri, A.; Noorollahi, Y.; Moosavian, S.F. Multi-Criteria Decision for Selecting a Wind Farm Location to Supply Energy to Reverse Osmosis Devices and Produce Freshwater Using GIS in Iran. *Energy Strateg. Rev.* **2023**, *45*, 101018. [[CrossRef](#)]
70. Anderson, M.B.; Milborrow, D.J.; Ross, J.N. Performance and Wake Measurements on a 3 M Diameter Horizontal Axis Wind Turbine. Comparison of Theory, Wind Tunnel and Field Test Data. In *Proceedings of the International Symposium on Wind Energy Systems*, Stockholm, Sweden, 21–24 September 1982; Volume 2, pp. 113–135.

71. Manwell, J.F.; McGowan, J.G.; Rogers, A.L. *Wind Energy Explained: Theory, Design and Application*; John Wiley & Sons: New York, NY, USA, 2010; ISBN 9780470015001.
72. Tang, Y.; Chang, Y.; Li, K. Applications of K-Nearest Neighbor Algorithm in Intelligent Diagnosis of Wind Turbine Blades Damage. *Renew. Energy* **2023**, *212*, 855–864. [[CrossRef](#)]

**Disclaimer/Publisher’s Note:** The statements, opinions and data contained in all publications are solely those of the individual author(s) and contributor(s) and not of MDPI and/or the editor(s). MDPI and/or the editor(s) disclaim responsibility for any injury to people or property resulting from any ideas, methods, instructions or products referred to in the content.